Microsc. Microanal. 18, 628–637, 2012
doi:10.1017/S1431927612000207

Microscopy AND Microanalysis

Spatial Resolution Optimization of Backscattered Electron Images Using Monte Carlo Simulation

Camille Probst,[1] Hendrix Demers,[1,2] and Raynald Gauvin[1,*]

[1]*McGill University, Mining and Materials Engineering, Montréal, Quebec H3A 2B2, Canada*
[2]*Universite de Sherbrooke, Electrical and Computer Engineering Department, Sherbrooke, Quebec J1K 2R1, Canada*

Abstract: The relation between probe size and spatial resolution of backscattered electron (BSE) images was studied. In addition, the effect of the accelerating voltage, the current intensity and the sample geometry and composition were analyzed. An image synthesis method was developed to generate the images from backscattered electron coefficients obtained from Monte Carlo simulations. Spatial resolutions of simulated images were determined with the SMART-J method, which is based on the Fourier transform of the image. The resolution can be improved by either increasing the signal or decreasing the noise of the backscattered electron image. The analyses demonstrate that using a probe size smaller than the size of the observed object (sample features) does not improve the spatial resolution. For a probe size larger than the feature size, the spatial resolution is proportional to the probe size.

Key words: backscattered electron, electron microscopy, Monte Carlo simulation, probe size, secondary electron, signal-to-noise ratio, spatial resolution

Introduction

Modern scanning electron microscopes (SEM) are equipped with more detectors than classical SEM and often the detectors are more complex. They are not limited to just the basic signals such as backscattered electron, secondary electron, and X-rays. For example, the transmitted electron signal can be detected with a special detector or/and specimen holder in a SEM (Bogner et al., 2007; Probst et al., 2007). A SEM image contains information from the analyzed sample, but the contrast mechanism has to be known to correctly interpret the image. The SEM user is faced with the problem of selecting the appropriate detector to obtain the best image and the information about the sample needed for the analysis. The spatial resolution can be used to compare quantitatively the images obtained from different detectors or instrument parameters to guide the user in the selection of the detector. One example is the evolution of spatial resolution with probe size for different instrument parameters and sample configurations, which is not well understood.

The spatial resolution measures the convolution of the object size, probe size, and interaction volume size. Many methods are available to measure or estimate the spatial resolution such as sharp edge or particle separation (Joy, 1974; Reimer, 1998; Goldstein et al., 2003). Another method to measure the spatial resolution using Fourier transform (FT) was developed and published as the Scanning Microscopy Analysis and Resolution Testing for ImageJ software (SMART-J) plug-in (Joy, 2002; Kim et al., 2007). The FT method was used to study the image sharpness in SEM (Postek & Vladár, 1998; Vladár et al., 1998; Zhang et al., 1999). A quantitative study of parameters influencing the spatial resolution in a SEM image is needed to first understand the spatial resolution obtained with the SMART-J method. We used this method in a previous study to compare different detectors and the effect of the working distance on images of carbon nanotubes (Probst et al., 2007).

The Monte Carlo technique is a great tool to exhaustively study many parameters that are difficult and time-consuming to obtain experimentally. Monte Carlo simulation was used to study the effect of backscattered electrons on spatial resolution in scanning Auger electron microscopy (El Gomati & Prutton, 1980). The resolution was not affected by increasing the accelerating voltage but only high energies (20 to 60 keV) were studied in that work. In another study, the spatial resolution of backscattered electron images for multilayer samples was calculated by Monte Carlo (Govoni et al., 1995; Merli et al., 1995). Also, the effect of the electron beam and backscattered electron detector characteristics on backscattered electron images were studied qualitatively by Monte Carlo simulation (Radzimski & Russ, 1995). Image simulation from Monte Carlo line scans was developed for critical dimension metrology applications (Postek et al., 2002). Monte Carlo simulation was also used to calculate the contrast of platinum particles in a carbon matrix when changing particle size, depth, and incident angle of the primary beam (Yue et al., 2005). The Monte Carlo simulation of scanning electron images was used to study gold nanoparticles on carbon substrates and to compare the resolution obtained with the gap and contrast-to-gradient methods (Mao & Ding, 2010). An analog image simulator, like the National Institute of Science and Technology Artimagen, is another possible method for image simulation (Cizmar et al., 2007, 2008*a*, 2008*b*).

Received July 18, 2011; accepted January 24, 2012
*Corresponding author. E-mail: raynald.gauvin@mcgill.ca

In this work, the spatial resolution of simulated backscattered electron images was obtained with the SMART-J method for different probe sizes, accelerating voltages, sample configurations (feature size and composition), and current or pixel dwell times (image acquisition time). The backscattered electron signal was chosen because it is easy to obtain and accurately described by Monte Carlo simulation. A description of the SMART-J method to calculate the spatial resolution is followed briefly by the Monte Carlo method used to generate the backscattered electron line scan. Next, the backscattered electron images are synthesized from the line scan. Finally, results of the spatial resolution versus probe size for these images at different instrument parameters and sample configurations show that using a probe size smaller than the size of the observed object (sample features) does not improve the spatial resolution. For probe sizes larger than the feature size, the spatial resolution is proportional to the probe size.

Methods

Simulated scanning electron microscopy images were created to understand the influence of the sample configuration and microscope parameters on the spatial resolution. The images were created from backscattered electron lateral line scans simulated with CASINO and the spatial resolution was estimated with SMART-J.

Spatial Resolution Measurements

The spatial resolution measurements made in this work used a modified version of the SMART-J (Kim et al., 2007) plug-in running in ImageJ software (http://rsbweb.nih.gov/ij/download.html). SMART-J uses the same algorithms as SMART macro (Joy, 2002), but it was written in java as an ImageJ plug-in. The plug-in uses the FT of the image to calculate the resolution by separating the contribution of the signal (object) and the noise in the FT image.

The plug-in needs the width of the image in micrometers. Once the size is entered, the FT of the region of interest is computed to obtain the corresponding power spectrum, which is displayed with a logarithmic intensity scale. In this work, the region of interest was fixed to 512×512 pixels for each measurement. The FT image is transformed into a binary image by applying a threshold transformation. The transformation allows the separation of the signal (center of the power spectrum) and the noise contribution.

The threshold value can be either selected by the user or obtained from the autothreshold method of ImageJ. In this work, we follow the suggestion of SMART macro authors (Joy, 2002) and select the threshold value when the cross-pattern just vanishes. The choice of the threshold value was user dependent, and different values were obtained with different users. The main effect of different users on a series of measurements was to bias the resolution results in one direction, i.e., one user systematically obtained higher values than another user. All resolution measurements in this study were obtained by the same user. Also, the SMART-J plug-in was modified to analyze a series of images, one after another with a minimum time between each image, which minimizes the judgment error from the user.

The error (standard deviation) for each spatial resolution value was estimated to be less than 5% by calculating the standard deviation for two series of 20 images with the same parameters. The series consisted of a 2 nm wide carbon layer in a gold matrix for a probe size of 2 and 10 nm with an accelerating voltage of 10 keV, a probe current of 1 pA, and a pixel dwell time of 114.4 μs (image acquisition time of 30 s).

Line Scan Simulations

The sample configuration used in this work was one small vertical layer with a width y (nm) embedded in a matrix of different composition as show in Figure 1A. The sample parameters that varied for this configuration are the layer width y (nm) and the composition of the layer and matrix.

For each parameter configuration, the beam position steps chosen for simulation have to be small to get enough information particularly in the middle of the sample (layer), and the simulated range has to be large enough to be outside of the observed layer. These two requirements give a larger number of points to simulate. To minimize the number of simulated points, three ranges were chosen. For all line scans created, three ranges of data were generated in the specific sample chosen: -300 to 300 nm (step size of 30 nm), -30 to 30 (step size of 3 nm), and -5 to 5 nm (step size of 0.5 nm) as shown in Figure 1A. For each beam position, backscattered coefficients were simulated, and the results of these three line scans were merged into one line scan.

The first version of CASINO Monte Carlo software was developed in 1997 (Hovington et al., 1997*a*) to simulate electron trajectories of specific samples inside an electron microscope. Version 2.42 was used in this work (http://www.gel.usherbrooke.ca/casino/index.html) (Drouin et al., 2007) to calculate the backscattered coefficients at specific beam positions in a vertical layered sample. The algorithms and models used in CASINO are detailed elsewhere (Joy, 1995; Drouin et al., 1997, 2007; Hovington et al., 1997*a*, 1997*b*). The elastic electron cross section of Mott (Czyzewski et al., 1990) was used to obtain the most accurate backscattered electron coefficient values. The probe size was chosen to correspond to the full-width at half-maximum (FWHM) of two-dimensional (2D) Gaussian distribution where the FWHM contains 76.1% of the incident electrons (Williams & Carter, 1996).

In Figure 1B, an example of a backscattered electron line scan is shown for which 100,000 electrons were simulated for each beam position. For this number of electrons, the simulation error is small compared to the backscattered coefficient values as shown in Figure 1B. For each set of backscattered coefficient measurements, it was possible to modify the probe size and the accelerating voltage of the beam used in the simulations.

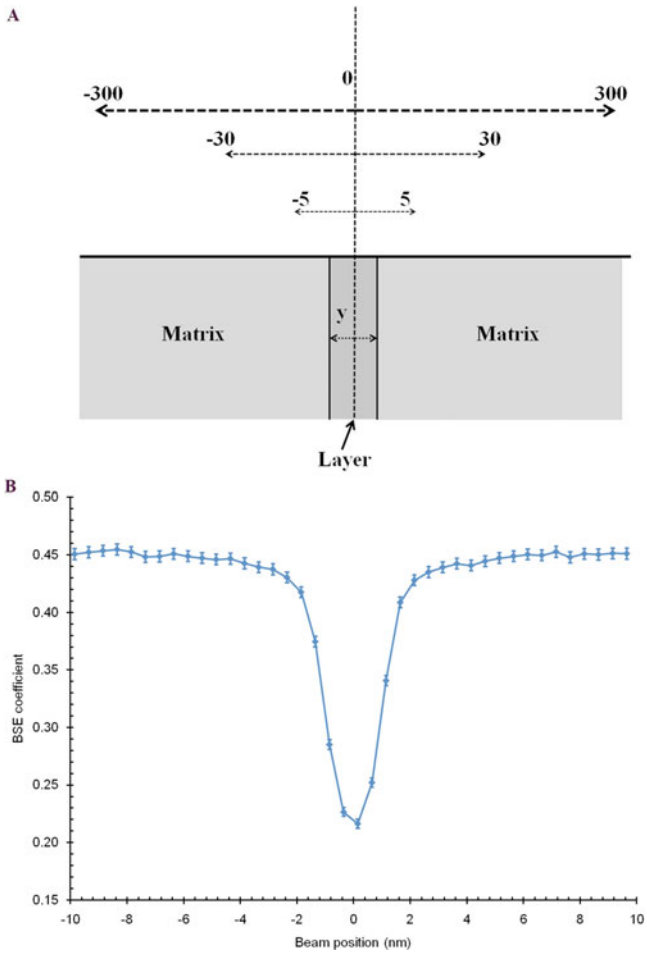

Figure 1. Backscattered electron coefficient line scans obtained with CASINO Monte Carlo program. **A:** Schematic of the sample configuration and the three beam position ranges (600, 60, and 10 nm) used. Each range has 21 beam positions, which gives a step size of 30, 3, and 0.5 nm, respectively. A vertical layer of lateral size y is embedded into a matrix of different composition. **B:** Example of a backscattered coefficient line scan for a 2 nm layer of carbon inside a gold matrix with a probe size of 2 nm and an accelerating voltage of 10 keV obtained with CASINO Monte Carlo software. The error bars show the Monte Carlo statistical error (3σ) associated with the simulation of 100,000 electrons used for each beam position.

Image Synthesis

The method used to calculate the spatial resolution in this work was developed for a complete image and not for a line scan. A Python (http://www.python.org/) script was used to generate a backscattered electron image from a simulated line scan.

Image size was fixed to 512×512 pixels corresponding to a scanning area of 120×120 nm^2. In addition, it was possible to modify probe current (I) and pixel dwell time (t) for each image by calculating the nominal number of electrons (N_0) for each pixel using this relation

$$N_0 = \frac{I \times t}{e}, \tag{1}$$

where e is the elementary charge of one electron.

The number of backscattered electrons, N_{BSE}, for each pixel in the image was obtained from the product of N_0 with backscattered coefficients η:

$$N_{BSE} = N_0 \times \eta. \tag{2}$$

Two methods were used to transform the line scan into an image. At first, simulated backscattered electron line scans were repeated horizontally to make a layered image. As explained before, the spatial resolution measurements are based on FT. FT of a linear layered image gives a perpendicular bar. With this kind of FT image, it was impossible to estimate spatial resolution with the SMART-J procedure.

In the second method, the image was synthesized by rotation of the simulated backscattered coefficients line scan to form a circular layer. The Monte Carlo statistical error created a backscattered electron image with a circular pattern. These circular patterns were also observed on the FT image. The FT enhances it because the same statistical errors were repeated in all directions due to the sample configuration, but the use of a circular layer permitted information in all directions. In the resulting FT, the part corresponding to signal was a disc, which was more adequate for SMART-J spatial resolution measurement.

Figure 2A is the backscattered electron image with a circular pattern and with electron gun shot noise added (Reimer, 1998). Electron gun shot noise corresponded to a

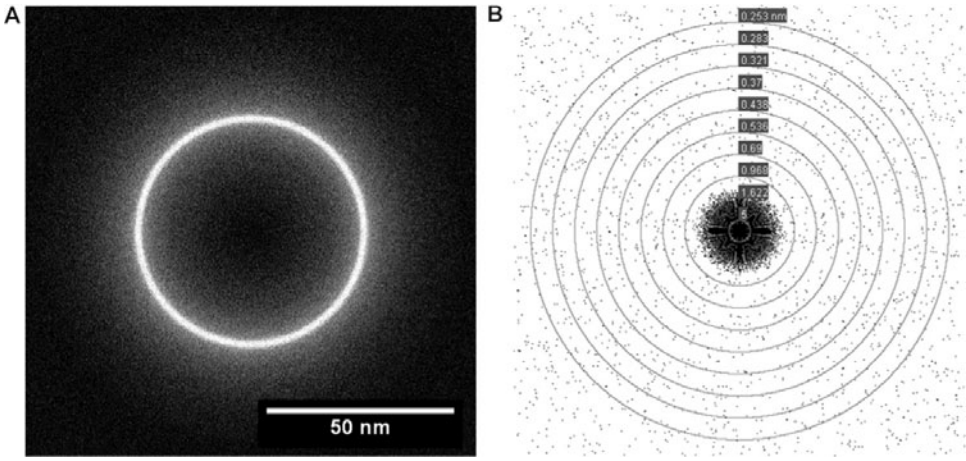

Figure 2. Example of spatial resolution measurement with the SMART-J method from a backscattered electron image. **A:** A circular gold layer with noise. **B:** The corresponding FT image. The backscattered electron image was obtained for a probe current of 1 pA and a pixel dwell time of 114.4 μs (image acquisition time of 30 s), which gives nominal number of electrons per pixel of 714. The image width is 120 nm.

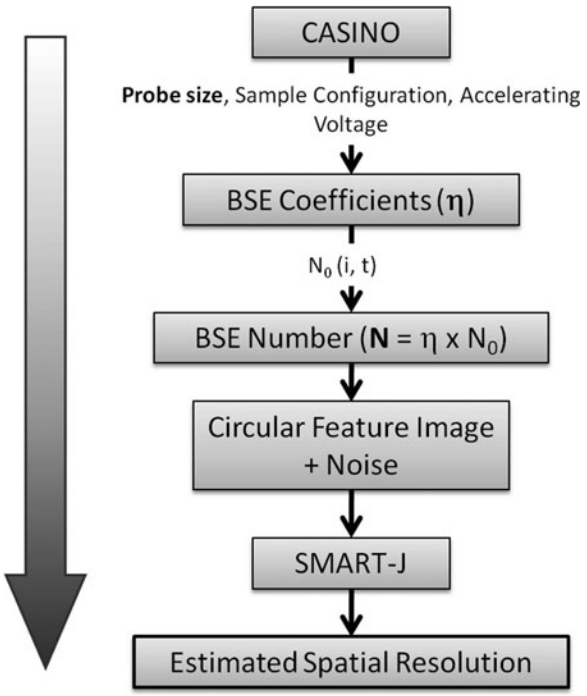

Figure 3. Diagram of the process used to generate backscattered electron images and to measure their spatial resolution.

normal distribution (Gaussian) with N_0 as mean value and variance equal to $\sqrt{N}$. The FT image obtained clearly shows that noise was larger than the Monte Carlo statistical error as the shot noise masks the circular patterns created by the Monte Carlo simulation (Fig. 2B). The shot noise is needed to calculate the spatial resolution, as the resolution is given by the transition between signal and noise in the FT image. The electron gun shot noise is not the only source of noise in a backscattered electron image (Reimer, 1998). A complete simulation of the noise effect has to include the backscattered electron emission statistic and the detector noise. This work focuses on the effect of probe size on the resolution. The omission of the other noise sources affects the absolute spatial resolution value calculated. However, the general observations described in this study are not affected by the exact simulation of the noise.

The validity of this method was verified by comparing the spatial resolution obtained with this method (line scan rotation to generate a 2D image) with a similar 2D image with each pixel directly simulated by Monte Carlo. No difference in spatial resolution between the two images was observed. Figure 3 summarizes the procedure used in this work to produce an image and measure the spatial resolution at different probe sizes and other parameters.

Results and Discussion

The backscattered coefficient (η) reflects the strength of the interaction of the incident electrons with the atoms of the sample. A heavier atom (higher atomic number) has a stronger electric potential, which causes the electron to deviate at greater angles resulting in smaller interaction volumes.

Figure 1B shows the variation of the backscattered coefficients with a beam position for a 2 nm carbon layer inside a gold matrix with an accelerating voltage of 10 keV and a probe size of 2 nm. Small variations of backscattered coefficient values in the matrix material (on left of line scan on Fig. 1B for example) were due to the simulation statistical error that depends on the number of simulated electrons (100,000 electrons). A quick change of backscattered coefficient was observed at the interface between the two materials, corresponding to a change of the relative atomic number of the interaction volume (Reimer, 1998; Goldstein et al., 2003). There are two extreme backscattered coefficient values that correspond to the value of the pure carbon (low value) and the pure gold (high value).

In Figure 1B, backscattered coefficient values at positions −10 (0.468) and 10 nm (0.470) were equal, within the simulation error, to the one of pure gold at 10 keV ($\eta_{Au} = 0.467$). In the center of the line scan (at the 0 nm position), a higher backscattered coefficient value (0.226) was obtained than the one of pure carbon ($\eta_C = 0.048$). The larger backscattered coefficient value is because the interaction volume at 10 keV in carbon, approximately 1 μm, is larger than the size of the carbon layer, 2 nm. If the probe size is larger than the layer width, a fraction of the electrons will interact with the matrix and not the layer, and the backscattered coefficient value will be influenced by the matrix composition. The backscattered coefficient value at center is lower than the one of pure gold because the interaction volume with a carbon layer is larger and deeper than the one for pure gold. The backscattered coefficient obtained at the center was a mix of carbon and gold.

Probe Size

The relation between spatial resolution and probe size was studied for a layer size of 2 nm and accelerating voltage of 10 keV for two elements: gold and carbon. Figure 4A shows the evolution of spatial resolution measured with SMART-J for various probe sizes. Results were obtained for a 2 nm carbon layer inside a gold matrix and the reverse sample configuration for an accelerating voltage of 10 keV, a probe current of 1 pA, and a pixel dwell time of 114.4 μs (image acquisition time of 30 s). Standard deviation of each measurement of spatial resolution obtained with SMART-J was found to be less than 5%.

A better spatial resolution (lower value) was obtained for the carbon layer inside the gold matrix sample than for the gold layer inside carbon for all probe sizes used. The difference in signal obtained from the two samples explains this difference. The signal S for each image or line scan was calculated using this equation

$$S = \eta_{max} - \eta_{min}, \quad (3)$$

where η_{max} is the maximum value of the backscattered coefficient in the image and η_{min} is the maximum value. For the sample configuration used in this work, the signal is given by the difference between the backscattered coefficient

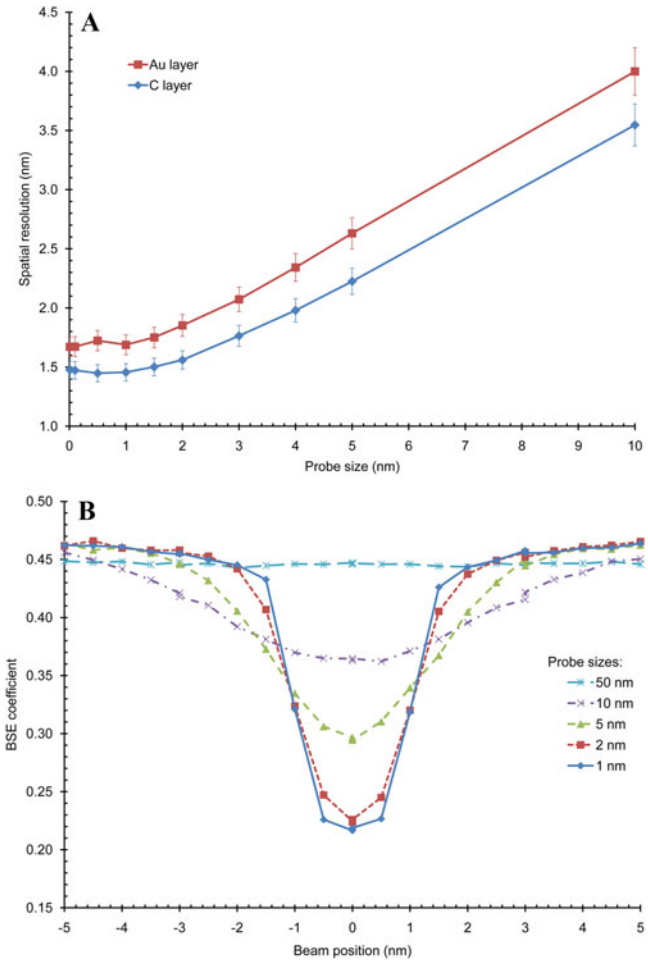

Figure 4. Evolution of spatial resolution as a function of the probe size. **A:** Two samples: a gold layer in a carbon matrix (Au-layer) and a carbon layer in a gold matrix (C-layer). An accelerating voltage of 10 keV and a layer of 2 nm were used. The probe current was fixed at 1 pA and a pixel dwell time of 114.4 μs (image acquisition time of 30 s) was used. The error bars show the standard deviation of 5% associated with each spatial resolution value. **B:** Backscattered coefficient line scans obtained for a 2 nm layer of carbon inside a gold matrix for an accelerating voltage of 10 keV for probe sizes of 50, 10, 5, 2, and 1 nm.

of the pure matrix and backscattered coefficient at the center of the layer.

The signals calculated for the carbon layer sample were always larger than the gold layer sample. For example, for a 2 nm probe size, the calculated signal of the carbon layer image was 0.252 and 0.166 for the gold layer. The signal difference was related to the higher backscattered coefficient and to the smaller interaction volume inside the gold specimen due to a larger number of elastic scattering events in gold than in carbon. For a carbon layer sample, the interaction volume size for a 2 nm layer is similar to the one for a pure gold, but the carbon layer has an elongate interaction volume that goes deeper into the sample and fewer electrons escape the sample, i.e., lower backscattered electron coefficient. It is difficult to predict the exact contribution for both components from the sample geometry. The compositions of the matrix and the layer influenced the calculated signal and spatial resolution.

In addition, Figure 4A shows that below a probe size of 2 nm, the spatial resolution reaches a minimum value independent of the probe size. The minimum resolution values obtained for the carbon layer were 1.5 and 1.7 nm for the gold layer. The minimum value obtained was close to the size of the object observed (layer size). Inversely, over this limit, spatial resolution was proportional to the probe size.

A better understanding of the effect of the probe size on spatial resolution can be obtained by studying the backscattered coefficient line scan. Figure 4B displays the simulated backscattered coefficients used to compute the backscattered electron image as a function of beam position in the range -5 to 5 nm, for probe size from 1 to 50 nm. The layer was a 2 nm carbon layer and the matrix was gold. Important variations of the backscattered coefficients at the middle of the layer were observed for probe sizes larger than 2 nm. Due to the small size of the carbon layer (2 nm), larger probe sizes gathered more information from the matrix. Smaller signal values were obtained because the increased probe size increases the backscattered coefficients in the middle of the layer, which resulted in a degradation of the spatial resolution. For probe sizes 2 nm and smaller, little variation was observed between the line scans.

Accelerating Voltage

In the previous section, we observed that the spatial resolution was affected by the interaction volume size, which is affected by the composition of the sample. Interaction volume for the same sample composition can be changed by varying the accelerating voltage.

Figure 5 shows the variation of the spatial resolution with the increase of probe size for different accelerating voltage and two sample compositions. The current was fixed to 1 pA and the pixel dwell time to 114.4 μs (image acquisition time of 30 s). Figure 5A displays results for a carbon layer of 2 nm inside a gold matrix, whereas Figure 5B shows results for a 2 nm gold layer inside a carbon matrix. The same probe size and layer composition effects described in the previous section were again observed. For all accelerating voltages (1, 10, and 30 keV) and both specimen compositions, the spatial resolution reached a minimum value below a probe size of 2 nm. Above 2 nm, the spatial resolution increases with larger probe size.

The spatial resolution value was also larger for higher accelerating voltages independent of the probe size or sample composition used. Increasing the accelerating voltage degrades the resolution of the backscattered electron image. This effect is clearly illustrated for the minimum value of the resolution observed for a probe size below 2 nm.

Figure 5C shows the size difference of the interaction volume for an accelerating voltage of 1 and 10 keV in a pure carbon sample. The interaction volume for an accelerating voltage of 1 keV was in the same order of the layer size (nanometer scale) and does not influence the spatial resolu-

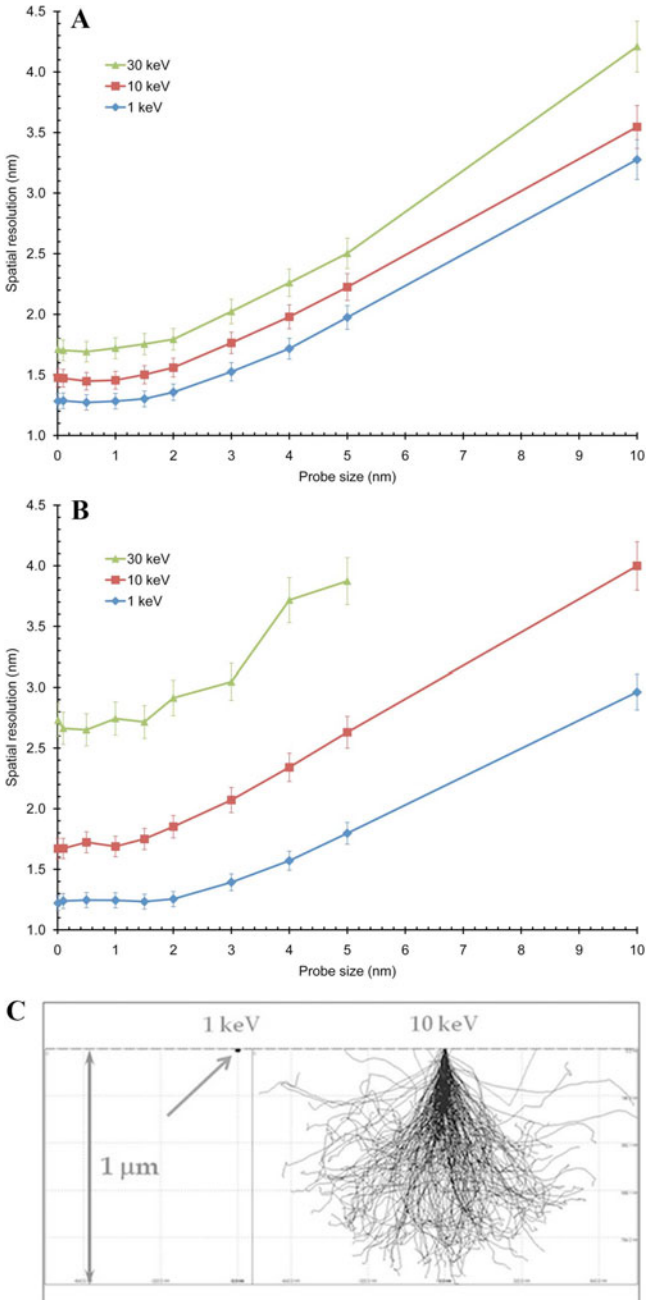

Figure 5. Variation of spatial resolution as a function of the probe size for accelerating voltages of 1, 10, and 30 keV. **A:** A carbon layer of 2 nm inside a gold matrix. **B:** A gold layer of 2 nm inside a carbon matrix. The probe current was fixed at 1 pA, and a pixel dwell time of 114.4 μs (image acquisition time of 30 s) was used. The error bars show the standard deviation of 5% associated with each spatial resolution value. **C:** Comparison of the interaction volume in a carbon sample at two accelerating voltages: 1 and 10 keV.

tion because even at 1 keV the interaction volume is larger than the smaller probe size. The size of the interaction volume increases with increasing accelerating voltage and at 10 keV in a pure carbon sample, it is approximately 1 μm. A similar effect is observed for gold, but the importance of the increase of the interaction volume with increasing accelerating voltage is smaller than the one for carbon, which explains why the increase of spatial resolution values for a gold matrix sample (Fig. 5A) was less important than for a carbon matrix (Fig. 5B).

The decrease of spatial resolution values with the reduction of accelerating voltage was due to condensation of the interaction volume at low voltage. Smaller interaction volumes in the middle of the layer lead to a larger fraction of the backscattered electrons coming from the layer itself and not from the matrix. This gives a backscattered coefficient closer to the one of the pure sample and, as explained before, gives a higher signal value and better spatial resolution at lower accelerating voltage for the same sample configuration.

The minimum spatial resolutions for a gold layer inside a carbon matrix were worse compared to the ones of a carbon layer in a gold matrix for 10 and 30 keV accelerating voltages. For 30 keV, 2.7 nm was obtained for a gold layer compared to 1.7 nm for a carbon layer. A carbon matrix has a larger interaction volume than a gold matrix, and this difference increases with larger accelerating voltage.

Finally, due to the small size of the layer and for a large interaction volume (matrix with low atomic number, high accelerating voltage), signals were smaller than the ones obtained for small interaction volume (matrix with high atomic number, low accelerating voltage), and spatial resolution falls. For example, signal was lower for an accelerating voltage of 30 keV ($S_{30} = 0.144$), a probe size of 2 nm and a 2 nm carbon layer inside a gold matrix compared to the one obtained at 10 keV ($S_{10} = 0.252$) or to the one obtained at 1 keV ($S_1 = 0.314$) as shown in Table 1.

A higher accelerating voltage increases the interaction volume, which degrades the spatial resolution. At the middle of the layer, the contribution of the matrix to backscattered coefficient is more important for larger interaction volume. The increase of interaction volume size is more important for lighter materials (low atomic number).

Nominal Number of Electrons per Pixel

As shown in equation (1), varying the probe current (I) or pixel dwell time (t) is equivalent to modifying the nominal

Table 1. Effect of the Accelerating Voltages on Image Signals and Spatial Resolutions.*

Matrix	Layer	Accelerating Voltages (keV)	Signal	Resolution (nm)
C	Au	1	0.349	1.3
Au	C	1	0.313	1.3
C	Au	10	0.166	1.9
Au	C	10	0.252	1.6
C	Au	30	0.057	2.9
Au	C	30	0.151	1.8

*Simulated values were obtained for a 2 nm layer and a 2 nm probe size, and for both gold and carbon sample configurations. Probe current was fixed at 1 pA and a pixel dwell time of 114.4 μs (image acquisition time of 30 s) was used.

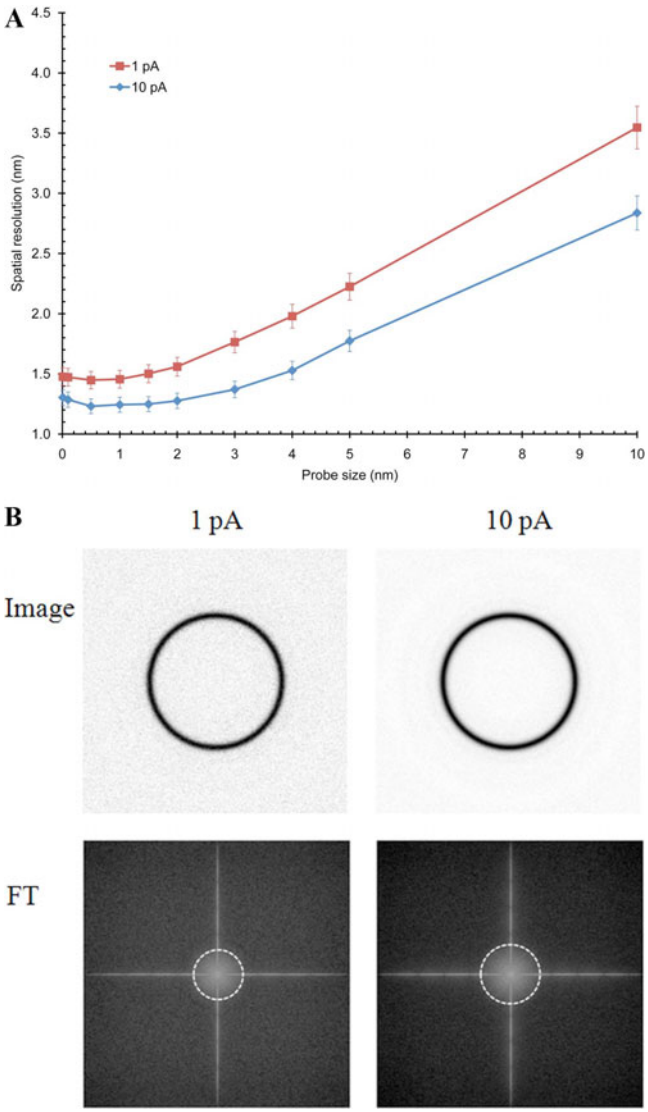

Figure 6. Effect of the probe current on the spatial resolution. **A:** Spatial resolutions were displayed as a function of probe sizes for two different probe currents (1 and 10 pA) and for a carbon layer inside gold matrix. The accelerating voltage was fixed to 10 keV, and a pixel dwell time of 114.4 μs (image acquisition time of 30 s) was used. The error bars show the standard deviation of 5% associated with each spatial resolution value. **B:** Backscattered electron images created for a 2 nm carbon layer inside gold matrix on top and their resulting FT images on bottom for a probe current of 1 pA (left) and 10 pA (right). The corresponding spatial resolution for each backscattered electron image is indicated by a dashed circle on the FT image. A spatial resolution of 2 nm was obtained for a probe current of 1 pA, and the spatial resolution decreases to 1.5 nm when the probe current increases at 10 pA. The accelerating voltage was fixed to 10 keV, the pixel dwell time to 114.4 μs (image acquisition time of 30 s), and the probe size to 4 nm.

number of electrons per pixel (N_0) and the number of backscattered electrons collected (N_{BSE}). Figure 6A displays the evolution of spatial resolution as a function of the probe size for two different probe currents: 1 and 10 pA, for a carbon layer inside a gold matrix. In this case, signal was constant because backscattered coefficients were constants.

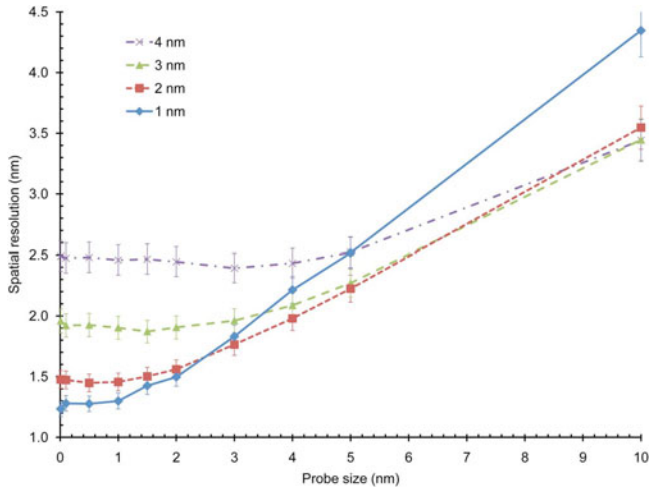

Figure 7. Influence of the carbon layer lateral size inside a gold matrix on the spatial resolution as a function of probe size. Images were created with an accelerating voltage of 10 keV, a probe current of 1 pA, and a pixel dwell time of 114.4 μs (image acquisition time of 30 s). The error bars show the standard deviation of 5% associated with each spatial resolution value.

A higher current gives better spatial resolution (lower value). The increased number of backscattered electrons collected improves the signal-to-noise ratio (SNR) (Reimer, 1998). The signal was proportional to N and the noise is proportional to $\sqrt{N}$; thus, the SNR was proportional to $\sqrt{N}$. This increase of SNR is observed in Figure 6B, where the 1 pA image has a noisier appearance than the one at 10 pA. Figure 6B also shows the resulting FT images showing the larger SNR with higher probe current. The disc at the center of the FT image corresponds to the signal. The size of the disk increases with a larger current. In a FT image, the pixels are inversely proportional to spatial dimension.

Increasing nominal number of electrons per pixel improved the SNR and gives a better spatial resolution. A spatial resolution of 1.3 nm was obtained with a probe current of 10 pA at 10 keV, which is the same resolution obtained at 1 keV with a probe current of 1 pA.

Layer Size

In the previous sections, a constant value of the resolution was obtained when the probe size was smaller than the layer size. The resolution variation with probe size was studied for different layer sizes to verify this correlation between layer size and probe size.

Figure 7 displays the variation of the spatial resolution with an increase of the probe size for different sizes of a carbon layer (1, 2, 3, and 4 nm) inside a gold matrix. The images were obtained with a probe current of 1 pA, a pixel dwell time of 114.4 μs (image acquisition time of 30 s), and an accelerating voltage of 10 keV. The value of the minimum spatial resolution varies depending on not only the layer size, but also the probe size limit when the minimum is reached depends of the layer size. This confirms that the spatial resolution is limited by the layer size

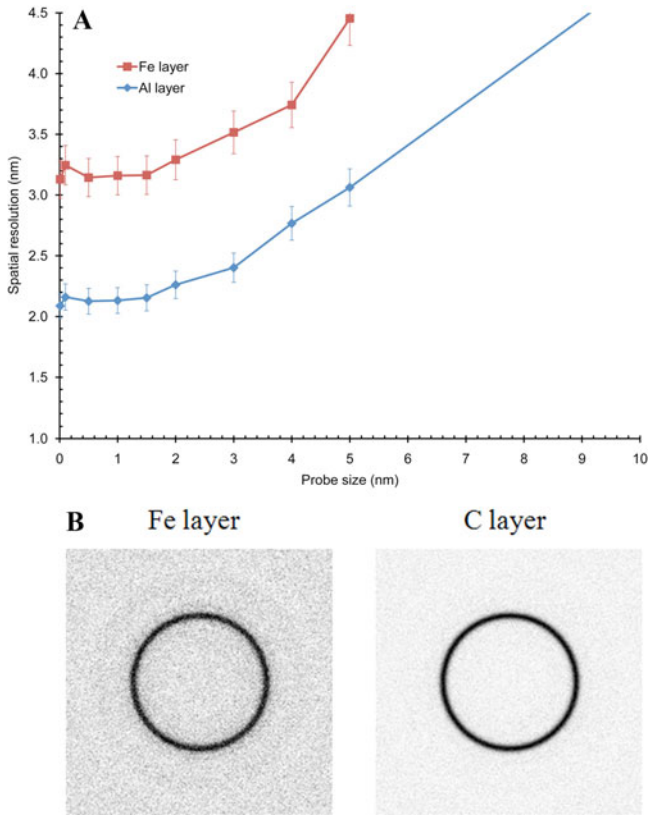

Figure 8. Effect of the sample composition on the spatial resolution of backscattered electron images. **A:** Evolution of spatial resolution as function of probe size for two samples: a 2 nm aluminum layer inside an iron matrix and a 2 nm layer of iron inside aluminum matrix. The probe current was fixed to 1 pA, the accelerating voltage to 10 keV, and the pixel dwell time to 114.4 μs (image acquisition time of 30 s). The error bars show the standard deviation of 5% associated with each spatial resolution value. **B:** Backscattered electron images created for a 2 nm layer of aluminum inside iron matrix on left and a 2 nm carbon layer inside a gold matrix on right. Images were computed with a probe size of 4 nm, a probe current of 1 pA, an accelerating voltage of 10 keV, and a pixel dwell time of 114.4 μs (image acquisition time of 30 s).

independently of probe size below a value close to the size of the layer.

A large increase in the spatial resolution of the 1 nm layer was observed compared to the others for a larger probe size. The signal falls with increasing probe size. As observed previously, lower signal results in larger spatial resolution (decreased resolution). For a small probe size of 1 nm, a signal of 0.203 was obtained for a 1 nm layer and 0.248 for a 2 nm layer. The spatial resolution was 1.3 and 1.5 nm, respectively. The reverse trend was observed for a probe size of 10 nm. The signal (resolution) was 0.085 (4.4 nm) for a 1 nm layer and 0.172 (3.5 nm) for a 2 nm layer.

The backscattered coefficients at extreme positions (inside the matrix) of the line scans were always equal to the one of pure gold (0.467). For the middle position (layer), backscattered coefficient values were dependent on the probe size and corresponded to a mixture of gold-carbon. Due to the small size of the layer (1 nm), bigger probe sizes gathered more information from the matrix at the middle position. For larger probe sizes, the backscattered coefficients obtained where closer to the one of gold, i.e., smaller signal and worst spatial resolution.

In summary, for small probe sizes, spatial resolution obtained depends mainly on the layer size. When the probe size is larger than the layer size, the resolution depends on both the probe size and the layer size.

Sample Composition

The simulations were repeated with another pair of elements to understand the impact of different composition on the spatial resolution. The elements used were aluminum (13) and iron (26). The smaller difference in atomic number indicates that the effect of different sizes of interaction volumes are smaller as shown by the backscattered coefficient values obtained at 10 keV: 0.157 for pure Al and 0.279 for pure Fe.

Figure 8A shows the variation of spatial resolution as a function of probe size for the aluminum and iron. The Fe layer curve corresponds to backscattered electron images of a 2 nm layer of iron inside an aluminum matrix. Conversely, the Al layer curve corresponds to a 2 nm aluminum layer inside an iron matrix. The accelerating voltage was fixed to 10 keV, the probe current at 1 pA, and the pixel dwell time to 114.4 μs (image acquisition time of 30 s).

Figure 8A confirms the results obtained previously with the carbon/gold samples for the dependence of the spatial resolution on the probe size: presence of minimum spatial resolution value at low probe size, increase with larger probe size and higher spatial resolution when the layer is a heavier material than the matrix compared to the reverse configuration.

Table 2 compares the signal and spatial resolution obtained for both sample compositions studied. The spatial resolution for both aluminum/iron configurations was always worse (higher spatial resolution value) than those obtained with carbon and gold. The lower signal for the couple aluminum/iron pair, as shown in Table 2, was due to their closer backscattered coefficients (η_{Al} = 0.157, η_{Fe} = 0.279 at 10 keV) in pure samples compared to carbon and gold (η_{C} = 0. 048, η_{Au} = 0.467 at 10 keV). Again, lower signal results in worse spatial resolution.

Table 2. Effect of the Sample Compositions on Image Signals and Spatial Resolutions.*

Matrix	Layer	Signal	Resolution (nm)
C	Au	0.166	1.9
Au	C	0.252	1.6
Al	Fe	0.054	3.3
Fe	Al	0.075	2.3

*Simulated values were obtained for a 2 nm layer and a 2 nm probe size for an accelerating voltage of 10 keV, a probe current of 1 pA, and a pixel dwell time of 114.4 μs (image acquisition time of 30 s).

Figure 8B shows a comparison of backscattered electron images obtained for the aluminum/iron and carbon/gold pairs. The iron layer in aluminum matrix image has a noisier appearance than the image for gold layer in carbon matrix. The lower signal as shown in Table 2 explains this noisier appearance for the same nominal number of incident electrons per pixel.

The spatial resolution was worse for smaller differences in atomic number. The smaller difference gives a poorer signal because the difference in backscattered coefficient values is small, which results in worse resolution.

Effect of Secondary Electrons

So far, the resolution was measured only for backscattered electron images. In the same experimental conditions, a secondary electron image should improve the spatial resolution because of the smaller emission volume (Reimer, 1998; Goldstein et al., 2003). The secondary electron emission is weakly dependent on the sample composition, and this dependence is from the secondary electron emitted by a backscattered electron. A greater secondary electron contrast is obtained when the sample has topographic features. The embedded layer sample used in the previous results does not offer topographic features. The sample illustrated in Figure 9A, which contains topographic features, was used to simulate high contrast secondary electron images. In this sample, a small cylinder, which replaces the smaller layer in the previous sample, is over a large, flat matrix.

CASINO (version 3.2) (Demers et al., 2011) was used to simulate backscattered and secondary electron line scans. From these line scans, an image was generated and the resolution was calculated with SMART-J using the same method described previously.

Variation of the spatial resolution with probe size is shown in Figure 9B for both backscattered and secondary electron images for a gold cylinder with a diameter of 2 nm on a carbon substrate. The accelerating voltage was fixed to 10 keV, the probe current at 1 pA, and the pixel dwell time to 114.4 μs (image acquisition time of 30 s). A better spatial resolution was obtained for the secondary electron images. Similar dependence on the probe size was observed for backscattered and secondary electron images. The resolution increased with larger probe size.

However, the presence of minimum spatial resolution at low probe size was not observed with this sample even for the backscattered electron images. The resolution was limited by the size of the layer for the previous sample. For a 2 nm cylinder, the small interaction volume for backscattered electrons is the limiting factor and not the size of the feature. Because the signal is maximal at the center of the cylinder (thicker) and decreases rapidly toward the cylinder edge (thinner), a smaller probe size will increase the maximum backscattered electron signal and gives a better resolution (lower value).

The contrast mechanism for a secondary electron image is completely different than for backscattered electrons. The secondary electron emission is very sensitive to the sample topography. For a cylinder sample, the maximum secondary electron emission occurs at the cylinder edge because most of the generated secondary electrons from the substrate escape the cylinder. However, the minimum emission occurs when the probe is on the substrate right after the cylinder edge because half of the emitted secondary electrons are absorbed by the cylinder. The cylinder edge is like a sharp knife edge, which is also a method to measure the probe size (Goldstein et al., 2003).

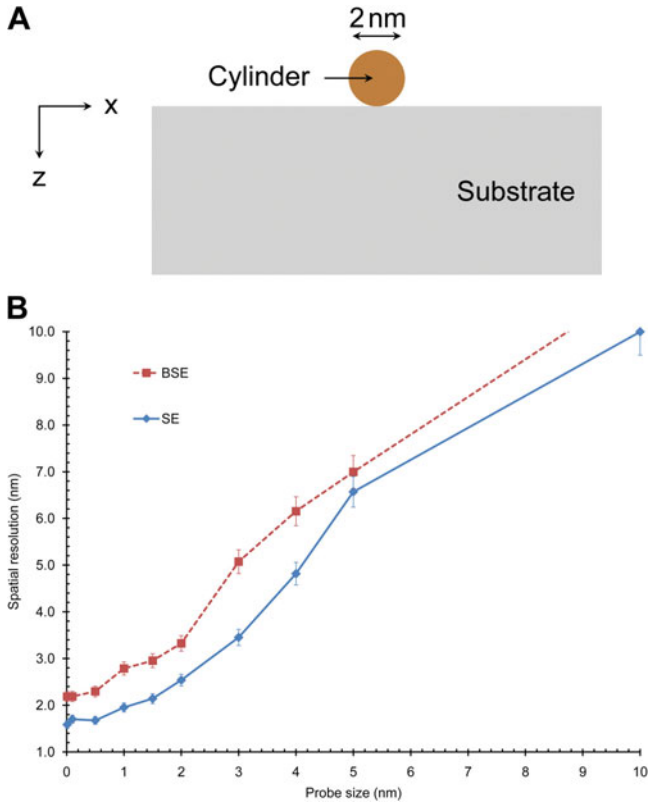

Figure 9. Comparison of the spatial resolution calculated from backscattered and secondary electron images for different probe sizes. **A:** Schematic of the sample configuration used. A gold cylinder of 2 nm diameter is on a carbon substrate. The electron beam was scanned in the *x* direction. **B:** Evolution of spatial resolution as a function of the probe size for backscattered and secondary electron images. The probe current was fixed to 1 pA, the accelerating voltage to 10 keV, and the pixel dwell time to 114.4 μs (image acquisition time of 30 s).

Summary

In this work, the spatial resolution of simulated backscattered electron images was calculated with SMART-J. The resolution was obtained by separating the signal and the noise in the FT image of the backscattered electron image.

The spatial resolution (lower value) can be improved by either increasing the signal or decreasing the noise. A higher current or pixel dwell time decreases the noise in a backscattered electron image. The signal is increased by a smaller probe size, a smaller accelerating voltage, and a larger difference in atomic number of materials used. However, these

improvements of the resolution are limited by the feature size of the sample (layer size). When the probe size is smaller than the feature size, the spatial resolution values are constant. For a probe size larger than the feature size, the spatial resolution is proportional to the probe size. However, the simulation of a small cylindrical feature shows that the interaction volume can also limit the spatial resolution. The simulations of secondary images have shown that the contrast mechanism can also be studied with this method.

When using an electron microscope all of these parameters are interdependent. The probe size increases with an increase of probe current or accelerating voltage. The maximum probe current is linked to the accelerating voltage or limited by specimen damage. Often the specimen configuration is fixed, and Monte Carlo simulations can help to find the optimum microscope conditions.

References

Bogner, A., Jouneau, P.H., Thollet, G., Basset, D. & Gauthier, C. (2007). A history of scanning electron microscopy developments: Towards "wet-STEM" imaging. *Micron* **38**(4), 390–401.

Cizmar, P., Vladár, A.E., Ming, B. & Postek, M.T. (2008*a*). Artificial SEM images for testing resolution-measurement methods. *Microsc Microanal* **14**(Suppl 2), 910–911.

Cizmar, P., Vladár, A.E., Ming, B. & Postek, M.T. (2008*b*). Simulated SEM images for resolution measurement. *Scanning* **30**, 1–11.

Cizmar, P., Vladár, A.E. & Postek, M.T. (2007). Image simulation for testing of SEM resolution measurement methods. *Scanning* **29**(2), 81–82.

Czyzewski, Z., MacCallum, D.O.N., Romig, A. & Joy, D.C. (1990). Calculation of Mott scattering cross section. *J Appl Phys* **68**(7), 3066–3072.

Demers, H., Poirier-Demers, N., Couture, A.R., Joly, D., Guilmain, M., de Jonge, N. & Drouin, D. (2011). Three-dimensional electron microscopy simulation with the CASINO Monte Carlo software. *Scanning* **33**(3), 135–146.

Drouin, D., Couture, A.R., Joly, D., Tastet, X., Aimez, V. & Gauvin, R. (2007). CASINO V2.42—A fast and easy-to-use modeling tool for scanning electron microscopy and microanalysis users. *Scanning* **29**(3), 92–101.

Drouin, D., Hovington, P. & Gauvin, R. (1997). CASINO: A new Monte Carlo Code in C language for electron beam interactions—part II: Tabulated values of the Mott cross section. *Scanning* **19**(1), 20–28.

El Gomati, M.M. & Prutton, M. (1980). Calculations of the effects of backscattered electrons upon the spatial resolution of the scanning Auger electron microscope due to changes in the primary energy and the angle of incidence. In *Electron Microscopy and Analysis, 1979*, Murlvey, T. (Ed.), pp. 361–364. London: The Institute of Physics.

Goldstein, J.I., Newbury, D.E., Echlin, P., Joy, D.C., Romig, A.D., Jr., Lyman, C.E., Fiori, C. & Lifshin, E. (2003). *Scanning Electron Microscopy and X-Ray Microanalysis: A Text for Biologists, Materials Scientists, and Geologists*. New York: Kluwer Academic/Plenum Publishers.

Govoni, D., Merli, P.G., Migliori, A. & Nacucchi, M. (1995). Resolution of semiconductor multilayers using backscattered electrons in scanning electron microscopy. *Microsc Microanal Microstruct* **6**(5–6), 499–504.

Hovington, P., Drouin, D. & Gauvin, R. (1997*a*). CASINO: A new Monte Carlo code in C language for electron beam interaction—part I: Description of the program. *Scanning* **19**(1), 1–14.

Hovington, P., Drouin, D., Gauvin, R., Joy, D.C. & Evans, N. (1997*b*). CASINO: A new Monte Carlo code in C language for electron beam interactions—part III: Stopping power at low energies. *Scanning* **19**(1), 29–35.

Joy, D.C. (1974). Measurement of SEM parameters. In *Proceedings of the 7th SEM Symposium*, Johari, O. (Ed.), Illinois Institute of Technology Research Institute, Chicago, pp. 327–334.

Joy, D.C. (1995). *Monte Carlo Modeling for Electron Microscopy and Microanalysis*. New York: Oxford University Press.

Joy, D.C. (2002). SMART—A program to measure SEM resolution and imaging performance. *J Microsc* **208**, 24–34.

Kim, J., Jalhadi, K., Lee, S.Y. & Joy, D.C. (2007). Fabrication of a Fresnel zone plate through electron beam lithographic process and its application to measuring of critical dimension scanning electron microscope performance. *J Vac Sci Technol B* **25**(6), 1771–1775.

Mao, S.F. & Ding, Z.J. (2010). A Monte Carlo simulation study on the image resolution in scanning electron microscopy. *Surf Interf Anal* **42**(6–7), 1096–1099.

Merli, P.G., Migliori, A., Nacucchi, M., Govoni, D. & Mattei, G. (1995). On the resolution of semiconductor multilayers with a scanning electron microscope. *Ultramicroscopy* **60**(2), 229–239.

Postek, M.T. & Vladár, A.E. (1998). Image sharpness measurement in scanning electron microscopy—part I. *Scanning* **20**(1), 1–9.

Postek, M.T., Vladár, A.E., Lowney, J.R. & Keery, W.J. (2002). Two-dimensional simulation and modeling in scanning electron microscope imaging and metrology research. *Scanning* **24**(4), 179–185.

Probst, C., Gauvin, R. & Drew, R.A.L. (2007). Imaging of carbon nanotubes with tin-palladium particles using STEM detector in a FE-SEM. *Micron* **38**(4), 402–408.

Radzimski, Z.J. & Russ, J.C. (1995). Image simulation using Monte Carlo methods: Electron beam and detector characteristics. *Scanning* **17**(5), 276–280.

Reimer, L. (1998). *Scanning Electron Microscopy: Physics of Image Formation and Microanalysis*. London, New York, Berlin: Springer.

Vladár, A.E., Postek, M.T. & Davidson, M.P. (1998). Image sharpness measurement in scanning electron microscopy—part II. *Scanning* **20**(1), 24–34.

Williams, D.B. & Carter, C.B. (1996). *Transmission Electron Microscopy: A Textbook for Materials Science*. New York: Plenum Press.

Yue, Y.T., Li, H.M. & Ding, Z.J. (2005). Monte Carlo simulation of secondary electron and backscattered electron images for a nanoparticle-matrix system. *J Phys D* **38**, 1966–1977.

Zhang, N.F., Postek, M.T., Larrabee, R.D., Vladár, A.E., Keery, W.J. & Jones, S.N. (1999). Image sharpness measurement in the scanning electron microscopy—part III. *Scanning* **21**(4), 246–252.